AN INVESTIGATION OF THE CHANNELLING OF PROTONS THROUGH THIN CRYSTALS

By

GRIFFIN F. HAMILTON
LIEUTENANT, UNITED STATES NAVY

A THESIS PRESENTED TO THE GRADUATE COUNCIL OF
THE UNIVERSITY OF FLORIDA
IN PARTIAL FULFILLMENT OF THE REQUIREMENTS FOR THE
DEGREE OF MASTER OF SCIENCE

UNIVERSITY OF FLORIDA

August, 1966

AN INVESTIGATION OF THE CHANNELLING OF PROTONS THROUGH THIN CRYSTALS

By

GRIFFIN F. HAMILTON
LIEUTENANT, UNITED STATES NAVY

A THESIS PRESENTED TO THE GRADUATE COUNCIL OF
THE UNIVERSITY OF FLORIDA
IN PARTIAL FULFILLMENT OF THE REQUIREMENTS FOR THE
DEGREE OF MASTER OF SCIENCE

UNIVERSITY OF FLORIDA

August, 1966

ACKNOWLEDGMENTS

The author desires to express his appreciation to his committee chairman, Dr. A. R. Quinton, for suggesting the topic and for his advice and encouragement in its development. Appreciation is also expressed to the other members of the Supervisory Committee, Dr. F. E. Dunnam and Dr. E. H. Hadlock. Messrs. Richard Prior and Juan Ramirez were of invaluable assistance in the preparation and conduct of the experiment. The constructive criticism offered by Assistant Professor M. Svonavec of Purdue University was especially valuable. Messrs. Robert Daniel and Kenneth Baker operated the Van de Graaff accelerator. Mrs. Pat Gates typed the manuscript. The author appreciates the faith and encouragement of Mrs. Griffin F. Hamilton and the United States Navy, without both of whose faith no success would have been possible. And a special note of appreciation is due Dr. S. S. Ballard, whose strong guiding hand ensures the continued excellence of Physics at the University of Florida.

TABLE OF CONTENTS

LIST OF TABLES

LIST OF FIGURES

CHAPTER I

INTRODUCTION

In the recent past, several investigators have taken under consideration the phenomena observed when charged particles interact with crystal lattices. Anomalous energy loss phenomena were first noticed in experiments on radiation damage in metals (1). Later reports cover several phenomena concerning the orientational dependence of reactions involving crystal lattices, including:

1) Non-uniform and orientationally dependent penetration of thick crystals (2,3);

2) Sharp orientationally dependent minima in large angle Rutherford scattering through thick crystals (4);

3) Dramatic departures from predicted nuclear reaction yields in thick crystals (5);

4) Non-smooth orientationally dependent angular distributions through thin crystals (6);

5) Anomalously large orientationally dependent energy losses in thin crystals (7); and

6) Anomalously low orientationally dependent energy losses of charged particles in thin crystals (8).

While all these phenomena can be roughly categorized as channelling effects (9), the use of the term "channelling"

has generally been restricted to the phenomenon of anomalously low energy losses of charged particles in thin crystals.

Charged particle channelling effects have been observed in silicon, germanium, and gold using protons (6,10,11), in germanium using deuterons (7), in gold using bromine and iodine ions (8), in aluminum using krypton ions and protons (2,3,11), and in copper using protons and krypton ions (11,12). In addition the slowing down of copper atoms in various lattice structures has been investigated by high-speed digital computer techniques (13).

The investigations forming the basis for this thesis were made using thin monocrystalline films of mica, silicon, and aluminum as targets for protons. The aluminum crystal was unsatisfactory, due to excessive thickness. Satisfactory results were obtained with the silicon crystal, although due to equipment limitations the effect observed was not as dramatic as has been elsewhere reported (9). The primary result of the investigations was the original observation of channelling in a multi-elemental crystal, mica. It is felt that this observation is of significance in the investigation of channelling.

CHAPTER II

THEORY OF CHANNELLING*

On entering a crystal along a direction of lattice symmetry (row or plane), energetic positively charged particles experience a coulomb repulsion from the atoms at the lattice sites. For critical impact parameters relative to the center axes of the arrays, the particles are scattered through such angles that they become collimated along those directions in the crystal where 1) repulsion forces from arrays on either side of the particle path are in approximate equilibrium, and 2) the electron density is relatively low. The trajectories of all other particles become random within a few collisions.

The theory of channelling is concerned basically with three predictions:

1) prediction of channelling orientations;

2) prediction of the limiting incidence angle for observable channelling; and

3) prediction of the magnitude of the energy anomaly.

---

*Due to the embryonic nature of channelling theory, no single authoritative source work exists. No attempt is made, therefore, to fully reference this chapter. Primary sources for this chapter are references 14 and 15.

Prediction of channelling orientations can be easily made through a basic knowledge of crystallography. Figure 1 shows the relationships between various planes and axes in a typical hexagonal close-packed crystalline lattice. Both silicon and mica exhibit this type of structure. In mica the (100) axis is perpendicular to the face of the crystal, but no such easy identification is available for silicon. The assumed orientation for silicon will be discussed in Chapter V.

The prediction of the limiting incidence angle for stable channelling proceeds as follows: A charged particle incident at angle Ψ to a symmetry array in a crystal has components of momentum both along the symmetry array (longitudinal) and normal to it (transverse). During the interaction, for small Ψ, the longitudinal momentum may be considered constant. The transverse momentum is $mv\Psi$, if Ψ is small, and the associated energy is $E_o\Psi^2$, where m and v are the mass and velocity of the incident particle and E_o is its total incident energy.

The transverse motion of a particle with this energy must be thought of as equivalent to a particle in an average potential field due to many atoms, for sufficiently large distances from the array.

If p_{min} represents the distance of closest approach of the particle to a row, then it satisfied the relationship

$$1-(u^2/p_{min}^2)-(\bar{V}(p_{min})^2/E\psi_o^2) = 0 \qquad (1)$$

where $\bar{V}(p_{min})$ is defined as the average row potential at a distance p_{min}, and u is the impact parameter of the interaction in a hypothetical plane perpendicular to the row on which is projected the trajectory.

If the particle trajectory is in the plane of the row of atoms, u = 0 and

$$E_o\psi^2 = \bar{V}(p_{min}) \qquad (2)$$

Thus the limiting incidence angle for stable channelling is defined, if the closest distance of approach is known. Although (2) is only correct in the extreme situation where u = 0, it is exact for an atomic plane where ψ is the angle of incidence of the particle to the plane. But defining p_{min}, and determining ψ, depend on the proper choice of a potential form. Table I shows average row and plane potentials for different interaction potentials V(r) between a charged particle and a single atom.

The determination of the magnitude of the channelling effect involves the definition of an anisotropy coefficient, F, as the fraction of the transmitted beam with anomalously low energy loss. An empirical formula for F is given by

$$F = 1-\exp\left\{-\left[\left(2\Phi/(\pi\,\bar{\theta}_t^2)^{\frac{1}{2}}\right)\,\left(\exp(-\psi^2/\bar{\theta}_t^2)\right)\right]\right\} \qquad (3)$$

where ψ is the angle of incidence to a planar channel, Φ is the half-angle of acceptance of the channel, and $\bar{\theta}_t^2$

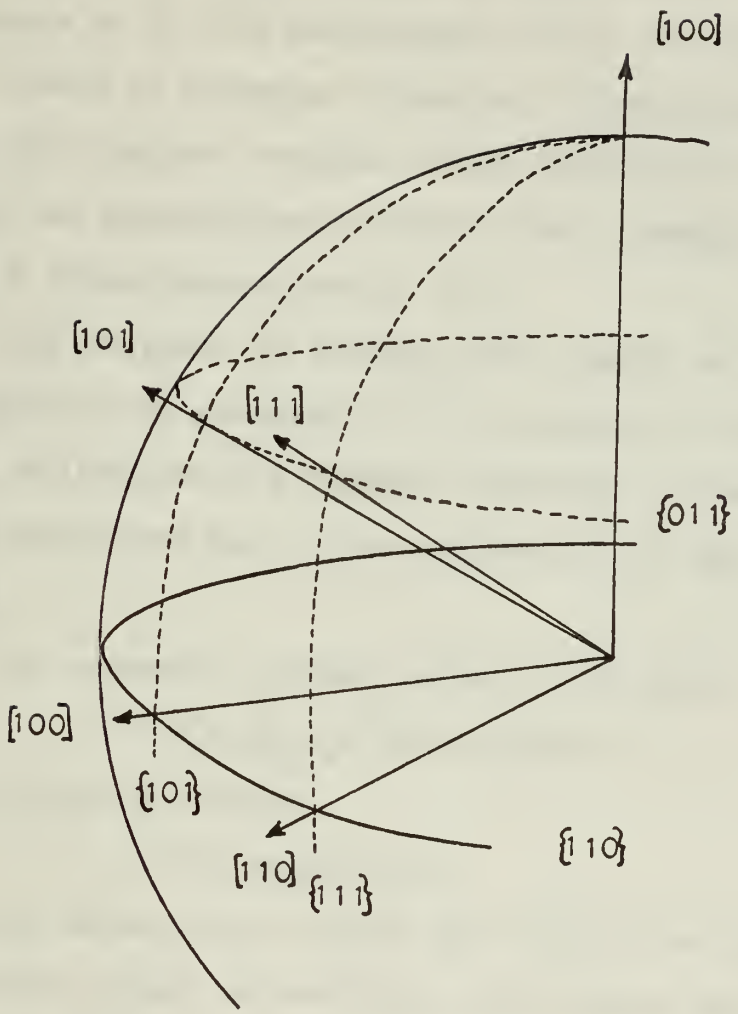

Figure 1

is the mean-square angle of multiple scattering through thickness t (14). For a given value of t the fraction F varies with ψ approximately as $\exp(-\psi^2/\bar{\theta}_t^2)$. Thus a slow decrease of F with increasing ψ is to be expected.

Table II compares values of F found experimentally here with values computed using equation (3). As can be seen, the comparisons indicate that equation (3) provides only a rough approximation of F.

The problems in fitting this theory to experimental data have been generally in the choice of a potential form, allowances for thermal vibration of the crystal, and aberrations due to non-uniformity of the potential field.

The screened coulomb potential of Bohr,

$$V(r)=(Z_p Z_t e^2/r)\exp(-r/a) \qquad (4)$$

and of Born and Mayer,

$$V(r)=A\exp(-r/a) \qquad (5)$$

are most often used, but neither gives good results over the entire range of particles and targets used in experiments to date. The conclusion may be drawn that a single potential expression valid for all cases would involve some combination of existing potential forms, with appropriate range form factors.

The effects of thermal vibration depend on the distribution of displacements about a lattice site. Assuming a Gaussian distribution with variance of $\overline{u_1^2}$ normal

Table I

Average row and plane potentials $\bar{V}(p)$ for different interaction potentials $V(r)$ between charged particle and single atom, where d is the row spacing, $1/A$ = atomic density in the plane, p= distance to row or plane, a_B = Bohr screening radius, a_{TF} = Thomas-Fermi screening distance, and $K_0(x)$ = zero-order modified Bessel function of the second kind (14).

Potential	$V(r)$	$\bar{V}(p)$(row)	$\bar{V}(p)$(plane)
Coulomb	$V(r)=Z_1Z_2e^2/r$	$\bar{V}(p)\cong(2Z_1Z_2e^2/d)\ln(d/p)$	$\bar{V}(p)\cong Z_1Z_2e^2/2\sqrt{A}$ for $p<\sqrt{A}$
Bohr's Screened Coulomb	$V(r)=(Z_1Z_2e^2/r)\exp(-r/a_B)$	$\bar{V}(p)=(2Z_1Z_2e^2/d)K_0(p/a_B)$	$\bar{V}(p)=(2Z_1Z_2e^2a_B/A)\exp(-p/a_B)$
Nielson's approximation to screened coulomb	$V(r)=Z_1Z_2e^2a_B/2r^2$	$\bar{V}(p)=Z_1Z_2e^2a_B/2pd$	$\bar{V}(p)\cong(Z_1Z_2e^2a_B/2A)\ln(A/4p^2)$
Moliere's approximation to Thomas-Fermi Potential	$V(r)=(Z_1Z_2e^2/r)[0.1\exp(-6r/a_{TF})+0.55\exp(-1.2r/a_{TF})+0.35\exp(-0.3r/a_{TF})]$	$\bar{V}(p)=(2Z_1Z_2e^2/d)[0.1K_0(6p/a_{TF})+0.55K_0(1.2p/a_{TF})+0.35K_0(0.3p/a_{TF})]$	$\bar{V}(p)=(2Z_1Z_2e^2a_{TF}/A)[(0.1/6)\exp(-6p/a_{TF})+(0.55/1.2)\exp(-1.2p/a_{TF})+(0.35/0.3)\exp(-0.3p/a_{TF})$

to the particle trajectory, a Born-Mayer potential is transformed to

$$\bar{V}'(p)=\bar{V}(p)\ \exp(\bar{u}_1^2/2b^2) \qquad (6)$$

where b is some constant, and $\bar{u}_1^2$ is a function of the Debye temperature of the target. It is seen that $\bar{V}'(p)$ increases slightly with increasing temperature, leading to a corresponding increase in Ψ (14). No temperature-dependence studies have as yet appeared in the literature.

The foregoing discussion indicates that the theory of channelling is quite inadequate.

CHAPTER III

APPARATUS AND TECHNIQUES

Equipment

The proton beam used in this experiment was provided by a model KN-4000 Van de Graaff accelerator manufactured by the High Voltage Engineering Corporation. The accelerator is capable of providing protons of from 0.5 to 4.0 million electron volts energy at a maximum beam current of 400 microamperes.

The accelerator is mounted vertically so as to produce the beam heading downward. Directly below the accelerator is a ninety degree momentum analyzing magnet which deflects to the horizontal only those particles of a momentum corresponding to the desired energy.

This horizontal beam is focused down the beam tube by a quadrupole focusing magnet (See Figure 2). Two fixed tantalum collimators and an adjustable slit tantalum collimator provide additional definition of the beam spot on the primary target in the scattering chamber.

The scattering chamber is an aluminum cylinder, two feet in diameter and 10.5 inches high. The primary target holder is located vertically on the axis of the

chamber. A target mounted on the target holder is thus directly in the path of the incoming beam. The vertical target may be rotated through 360° about a vertical axis without disturbing the system vacuum.

In the sides of the scattering chamber are ten two-inch diameter ports, to permit entry and exit of the beam, to attach the vacuum pumps, to measure inside pressure, and to permit observation of the primary target through clear windows. Unused ports are covered with blank brass plates. In this experiment a Faraday cup was fitted on the straight-through port, the channelling apparatus to be described was placed on the 45° (from straight-through) port, and all other ports, with the exception of the beam inlet port, were unused.

The Faraday cup collects the remnants of the beam passed through the primary target. The charge thus accumulated is measured by a current integrator, and this measurement is used to calculate the total amount of beam passing through the target. The amount of beam lost in the target due to scattering and nuclear reactions is negligible compared to the total beam because of the thinness of the primary target used.

The channelling apparatus (See Figures 3 and 4) affixed to the 45°-port on the scattering chamber consists of four sections. In order outward from the scattering chamber they are:

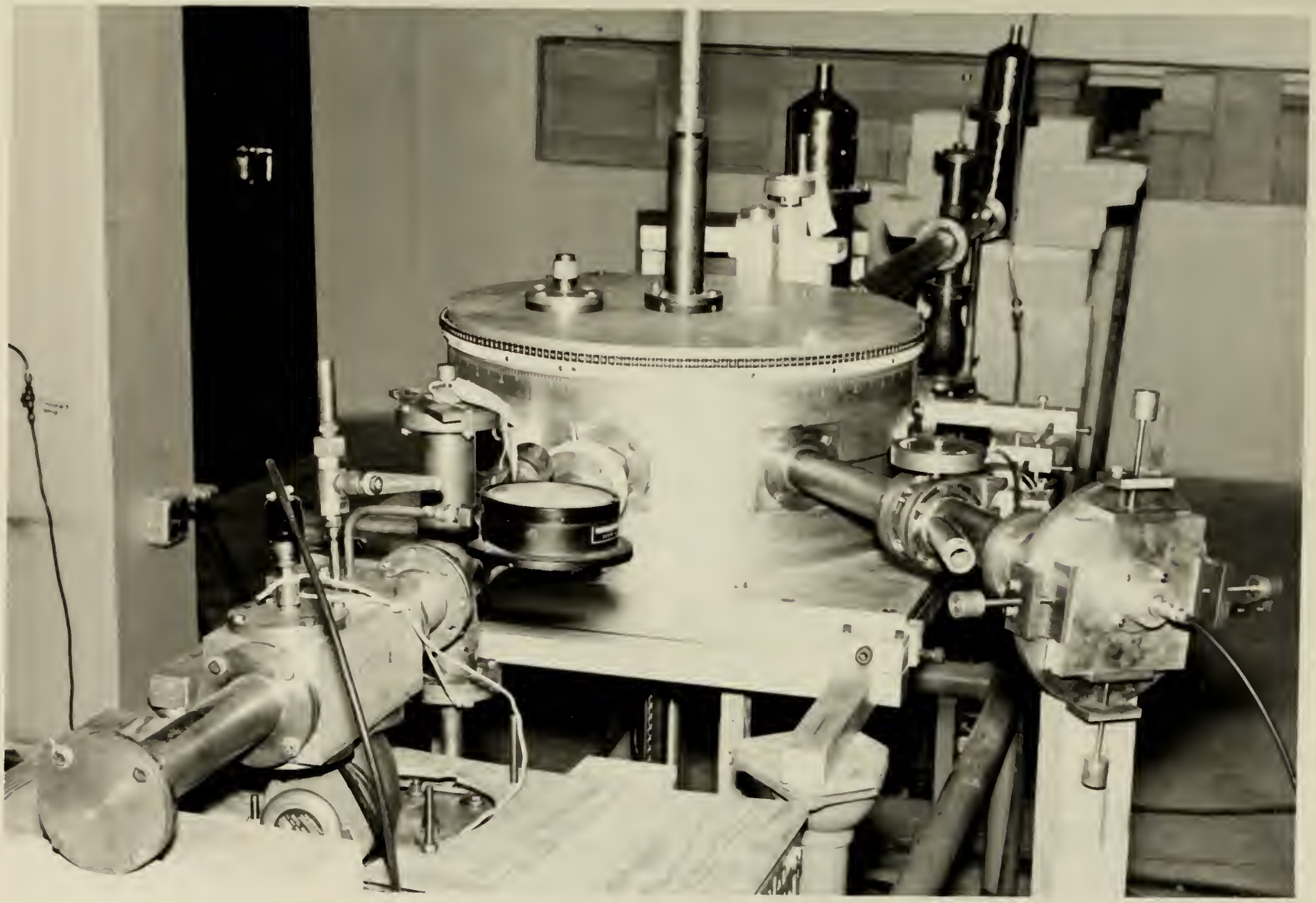

Figure 2

1) A ten-inch section of two-inch brass pipe;

2) A brass flange with a tantalum collimating disc mounted in its center;

3) A crystal target holder assembly; and

4) A detector and monitor assembly.

The ten-inch section of two-inch brass pipe assists in the collimation of the secondary beam by increasing the base line for beam dispersion calculations from 12.5 inches to 22.5 inches.

The brass flange supports the first collimating disc. This disc is a thin sheet of tantalum with a small collimating hole in the center. Four discs can be interchanged to give a hole size as small as 0.013 inch. In this experiment a 1/32-inch hole was found to be the smallest hole which would allow a sufficiently rapid counting rate. This size collimating hole 22.5 inches from a 1/8-inch diameter beam spot on the primary target gives a half-angle of dispersion on the secondary target of 0.1°.

The crystal holder assembly consists of a short length of two-inch brass pipe with a smaller brass tube inserted in its side normal to the axis. The crystal holder is mounted on a brass rod which moves inside this tube. A flange on the tube and a plate on the upper end of the rod have angular markings around their rims by which measurements of the angle θ to a relative

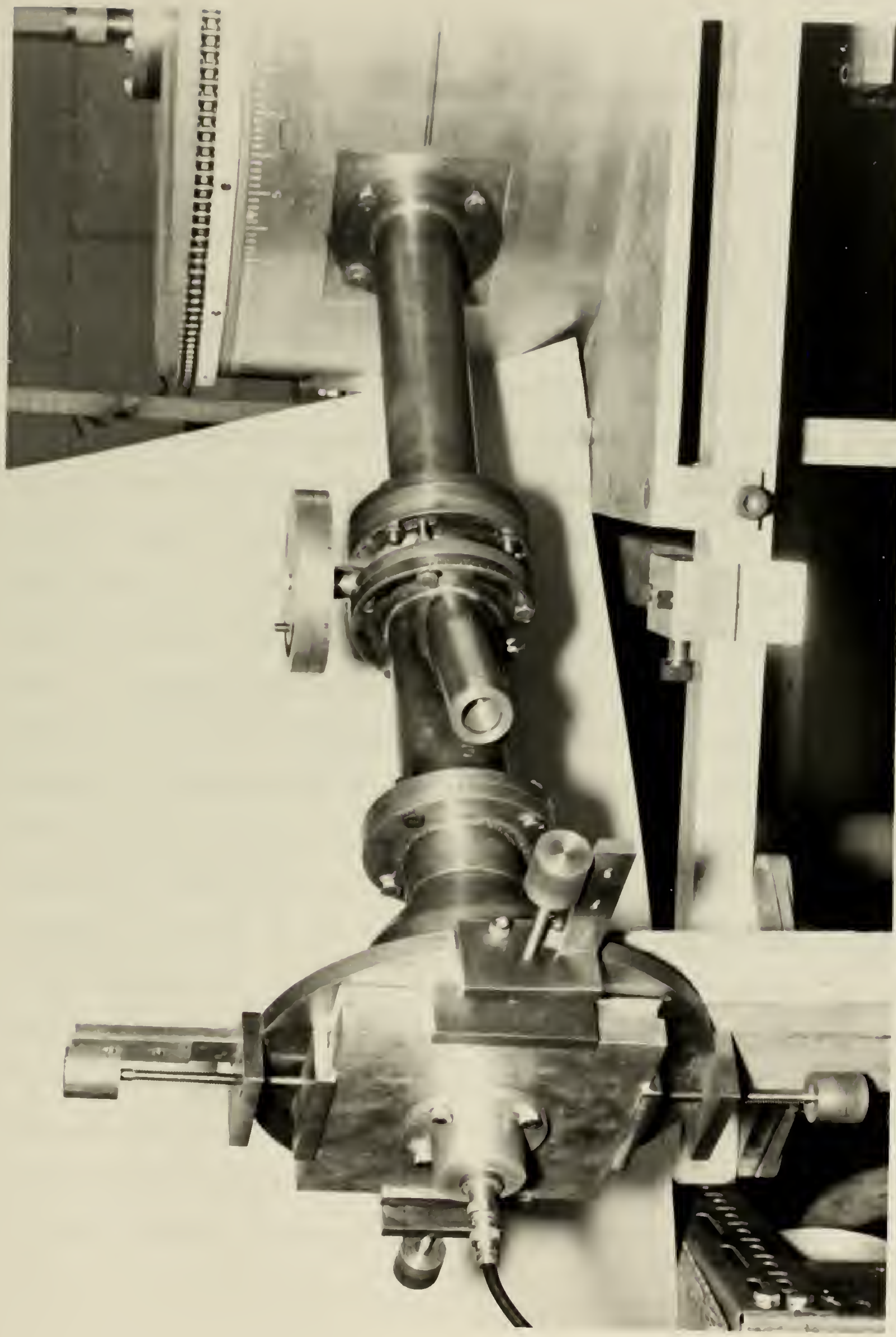

accuracy of 0.1° can be made. An O-ring on the rod allows adjustment of crystal position in θ without disturbing the system vacuum. The end flanges on the pipe also have angular markings on their rims, whereby the angle γ can be measured to a relative accuracy of 0.1°. Here again, with O-ring seals at either end, φ settings may be changed without affecting the system vacuum.

The detector and monitor assembly consists of an expanding diameter brass pipe nine inches long and open at the wide end, with two monitor detector ports mounted in the sides at the narrow end and a sliding plate over the open end. The two monitor detector ports are brass tubes placed at an angle of 25.2° with the beam axis, and so located that their axes converge at the target position when the crystal holder assembly is in place. Inside the brass tubes slide brass rods with provisions for mounting monitor detectors on their inner ends. The tubes are adjustable so that the detectors may be positioned as close as one inch or as far as five inches from the target. O-ring seals on the brass rods allow repositioning of the monitor detectors without breaking the system vacuum. In the sliding plate at the wide end are mounted the detector collimating device and the solid state detector. This plate allows the positioning of the detector in the X-Y directions normal to the beam

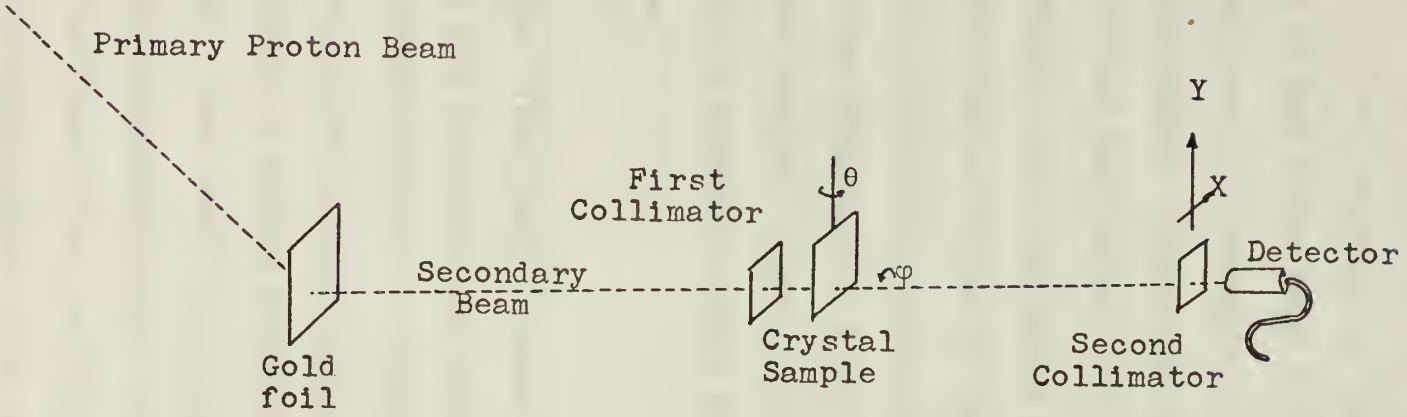
Primary Proton Beam
Y
First
Collimator
θ
X
Detector
Secondary
Beam
φ
Gold
foil
Crystal
Sample
Second
Collimator

Figure 4

path. The solid state detector is mounted in a recess in the center of the plate, with the collimating disc mounted one inch in front of it. This disc arrangement is identical in construction to the first collimating disc. Again it was found that a 1/32-inch hole was optimum. The plate is attached to the end of the assembly by four clamps, which are independently driven by screws. Two of the screws, as can be seen in Figure 3, are calibrated, and turn along a calibrated rule. By these screws the position of the sliding plate, and thus the second collimator and the detector, can be determined to an accuracy of 0.001 inch in X and Y. The solid state surface barrier silicon detector (ORTEC Model SBEJ025) is mounted behind the collimator on the sliding plate.

Electronics

The signals from the detector mounted on the sliding plate are fed into the low noise preamplifier section of an ORTEC Model 101 amplifier (See Figure 5). After being amplified in the preamplifier the signals are passed through a biased amplifier, which further amplifies them. The resulting signals are analyzed in a Nuclear Data Corporation Model ND-110 128-channel pulse height analyzer. The resulting analysis is displayed on a semi-logarithmic plot on a cathode ray tube, with number of counts as the ordinate and channel number

as the abcissa. Each channel in the analyzer represents an energy window in the spectrum.

By varying the gain and the bias on the biased amplifier the portion of the energy spectrum to be analyzed and the width of the individual energy windows may be varied.

Target Construction

As previously mentioned, thin monocrystalline mica, aluminum, and silicon targets were used.

Mica is readily obtainable in very thin, uniform sheets. Four targets were used, one of which was a commercial mica window. The other three were prepared by picking apart a "book" of pressed phlogopite mica ($KAl_3Si_3O_{10}(OH)_2$) with an ordinary straight pin and razor blade. The valuable feature of mica is that naturally occurring "books" of mica cleave along the base direction perpendicular to the (100) axis.

The preparation of the aluminum target involved electropolishing a cast aluminum plate to the desired thinness. A functional drawing of the apparatus for electropolishing is shown in Figure 6. The aluminum plate is used as one electrode, and an aluminum foil as the other. The proper electrolytic solution for electropolishing aluminum consists of one part nitric acid and four parts methanol. Since this mixture is explosive at room temperatures, it must be cooled with

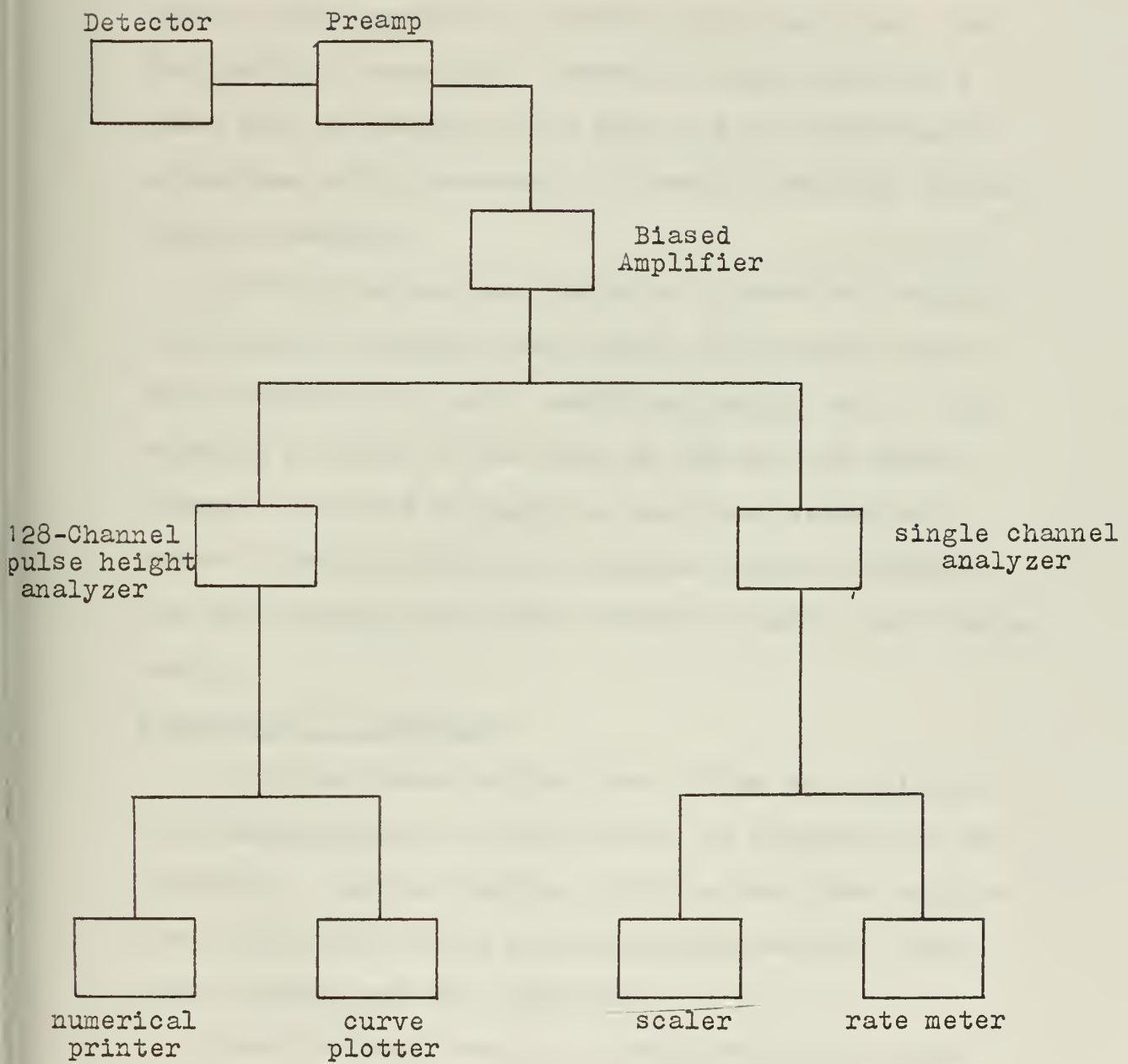
Detector
Preamp
Biased
Amplifier
128-Channel
pulse height
analyzer
single channel
analyzer
numerical
printer
curve
plotter
scaler
rate meter

Figure 5

dry ice. A potential of approximately six volts DC between the electrodes produces the desired effect, that is, the removal of aluminum from the plate. Unfortunately, successful electropolishing requires a great deal of practice, and time was not available to obtain the skills necessary to produce crystals of the thinness desired.

Silicon targets are prepared by chemical etching. The solution required consists of 85 ml nitric acid, 30 ml hydrofluoric acid, and 15 ml acetic acid. This solution polishes at the rate of one mil per minute. Extreme care must be taken in the final stages of either electropolishing or chemical etching, because the thin crystals have very little strength, and crumble easily.

Techniques of Operation

A system vacuum better than 10^{-5}mm Hg, monitored with thermocouples and ion gauges, is required for the operation. Special venting ports in the first collimator flange and in the detector plate assembly facilitate pumping out the apparatus.

When the main vacuum isolating valves have been opened, and the particle beam is directed into the scattering chamber, the beam spot size must be reduced to about 1/8 inch-diameter on the primary target. This

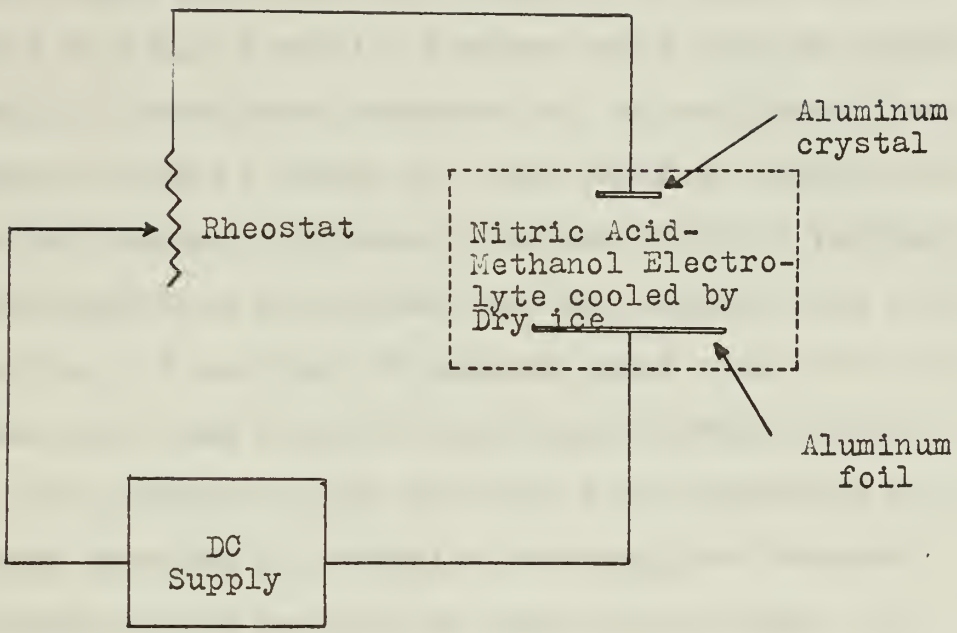
Aluminum crystal
Rheostat
Nitric Acid-Methanol Electrolyte cooled by Dry ice
Aluminum foil
DC Supply

Figure 6

is accomplished either by adjusting the movable slit collimators or by changing the field of the quadrupole focusing magnet.

Once the beam spot is as desired with the channelling target out of the beam path, the sliding plate is moved in X and Y until a maximum count rate is registered on a rate meter connected to the analyzer. Each time the beam is turned on, this position must be relocated because it changes with the slightly varying characteristics of the beam and the primary beam spot. When the X-Y position of maximum count rate has been found, the beam axis has been geometrically defined.

The taking of data involves first measuring an energy spectrum of particles reaching the detector without passing through the channelling target. By knowing the initial energy of such particles (from the settings on the momentum analyzing magnet), and their final energy, the energy loss in the first target can be determined. This determination facilitates the calculation of the effective thickness of the first target. Once the effective thickness is known, the specific energy loss of any type of particles at any incident energy can be found by calculation, or in most cases by consulting existing tables.

It must be noted that effective thickness depends also on the target orientation with respect to the

incident beam. Care must be taken to reproduce the orientation of the first target to within a few degrees each time, to minimize fluctuations in data.

After the relevant data without the second target have been obtained, the target is lowered into position, at an arbitrary angle of θ, where θ is the angle between the beam path and the normal to the crystal face. Several runs must first be taken at various angles of θ, to enable measurement of secondary target thickness. Target thickness, in energy units, is simply

$$t = (E_i - E_d) \cos \theta \qquad (7)$$

where E_i is the energy of particles incident on the second target and E_d is the energy of particles incident on the detector. Factors to convert t from units of energy to units of mg/cm^2 are readily available in tabular form (16). Correction of data for target thickness is an important step in the analysis of data.

The search for channelling in the target crystal involves taking data in 0.1^o or 0.2^o steps about 2^o either side of the predicted orientation. As previously noted, a single channel analyzer and a scaler count the total number of particles striking the detector on each run, thus providing normalization. At the conclusion of each run, the spectrum is recorded on a numerical print out and also on a curve tracer. The resulting curves are thus available for immediate comparison with

other runs.

Initial runs recorded 1000 counts on the scaler, for a statistical error of less than three percent. After the channelling orientation had been located, 10,000-count runs were taken at the channelling angle and at an orientation just beyond the limiting angle for observable channelling, to give a statistical error of the order of one percent.

CHAPTER IV

TREATMENT OF DATA

Treatment of data involved three distinct processes:

1) Selection of best raw data;

2) Application of corrections to best data; and

3) Selection of best display of results.

The selection of best raw data was made by direct comparison of the crude curves drawn by the curve plotter at the end of each run. This method was found to be more facile than comparisons of numerical readouts.

The data thus selected were corrected only for target thickness. As relatively little information on peak spreading due to multiple scattering or energy straggling in such cases is available, no attempt was made to correct for these effects. It is felt, however, that any contributions they might make would be small compared to the channelling effects observed, and would remain nearly constant through the small ranges of θ over which channelling was observed.

In order for the data to be useful the numerical print out in counts per channel must be converted to counts per energy increment. To accomplish this it was necessary to take a sequence of electronics-only runs,

using as a pulse source a calibrated pulse generator built into the amplifier. A representative graph of data taken is shown in Figure 7.

It was felt that a straightforward cartesian plot of results would be most meaningful. A semi-logarithmic plot shows a more pronounced high-energy shoulder, but has the effect of distorting the magnitude of the small effects observed.

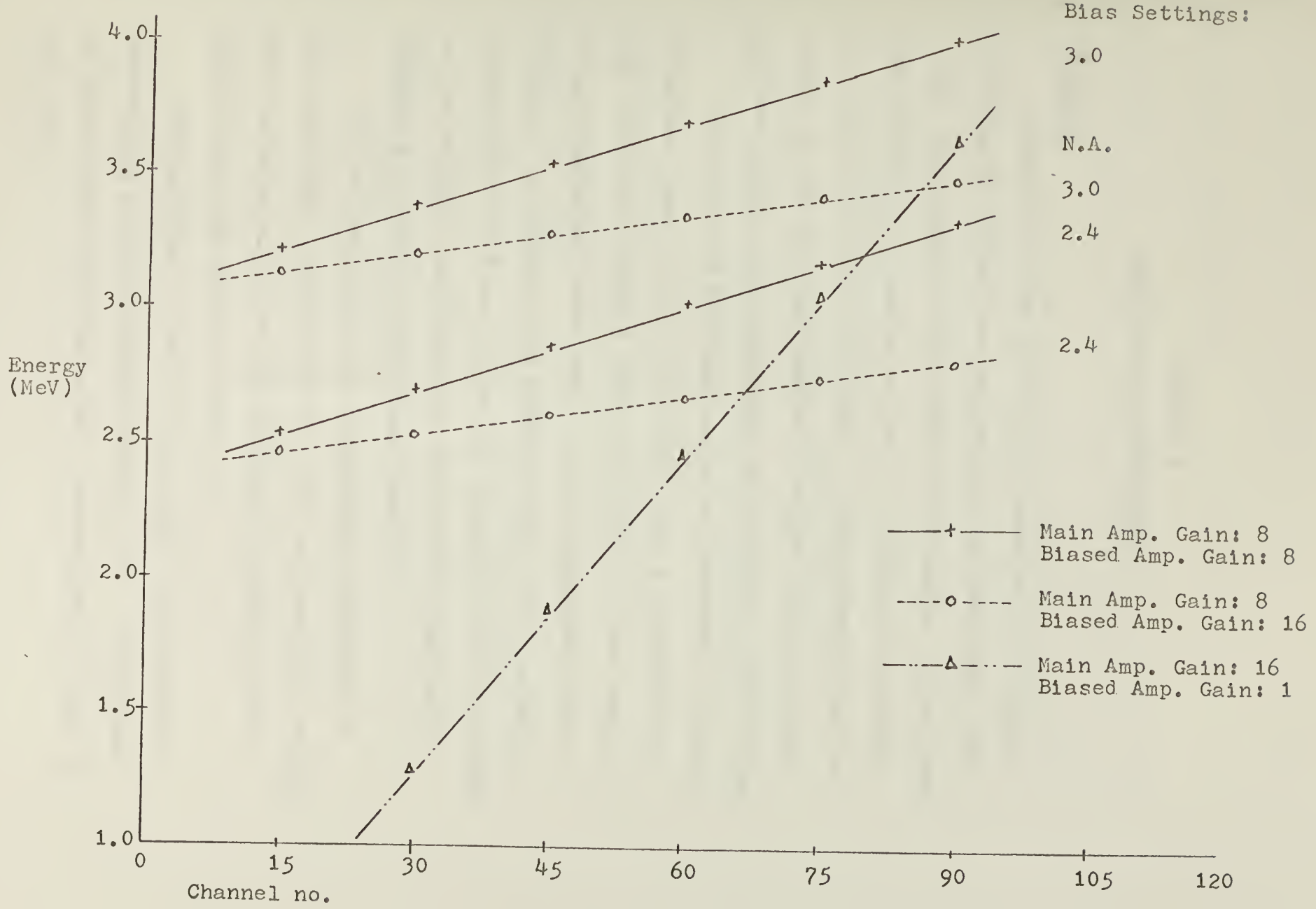
Bias Settings:
3.0
N.A.
3.0
2.4
2.4
Energy (MeV)
4.0
3.5
3.0
2.5
2.0
1.5
1.0
0
15
30
45
60
75
90
105
120
Channel no.
Main Amp. Gain: 8
Biased Amp. Gain: 8
Main Amp. Gain: 8
Biased Amp. Gain: 16
Main Amp. Gain: 16
Biased Amp. Gain: 1

Figure 7

CHAPTER V

RESULTS AND CONCLUSIONS

Results

Channelling was observed in mica and in silicon. In mica the effect was observed on, or very near, the (100) axis normal to the face of the sample. In silicon the effect was observed on the (111) plane at an angle of about 35° to the (100) axis. This determination was based on the axis information obtained from the source of the crystal, the department of Electrical Engineering.

In mica, the limiting angle for observable channelling was found to be $0.3^{\circ} \pm 0.05^{\circ}$, and 9.2 percent of the particles emerging from the crystal at the channelling orientation were found to have anomalously high energy. In silicon, the limiting angle for observable channelling was found to be $0.3^{\circ} \pm 0.05^{\circ}$, and 6.8 percent of the emergent particles had anomalously high energy. Figures 8, 9, and 10 show these results.

For both materials the anisotropy coefficient F was calculated (using equation (3)), and resulting values were compared with the experimentally obtained values. These values are shown in Table II.

Calculations of the limiting angle for observable channelling were made using equation (2). A comparison of these values with the actual observations is shown in Table III.

Table II

Anisotropy coefficient (F)

Material	F (predicted)	F (observed)
Mica	.181*	.092
Silicon	.363	.068

Table III

Limiting incidence angle for observable channelling

Material	predicted	observed
Mica	0.86°*	0.3°
Silicon	0.6°	0.3°

* Predictions in mica are based on an average Z at each lattice site of 10.42.

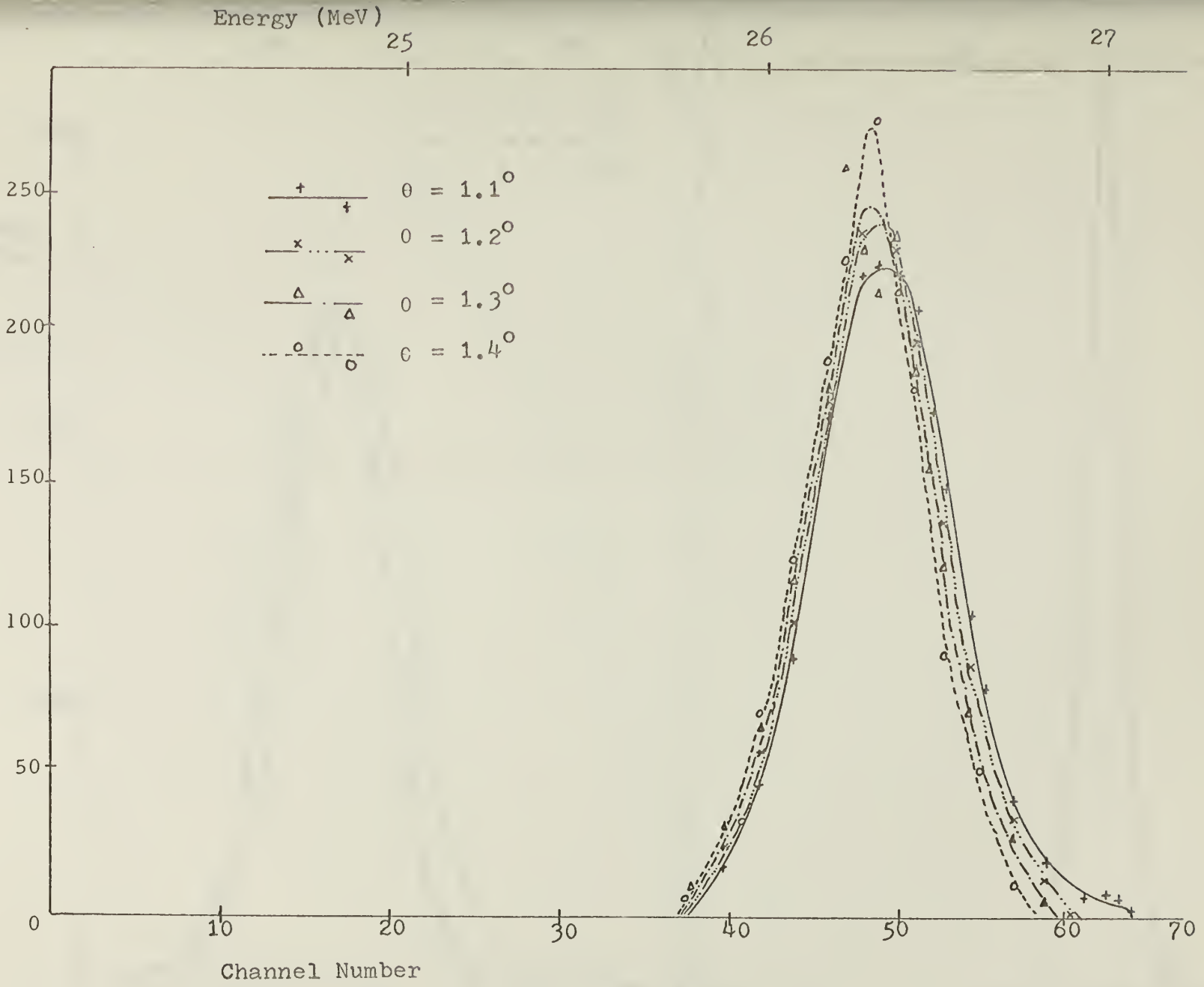
Energy (MeV)
25
26
27
θ = 1.1°
θ = 1.2°
θ = 1.3°
θ = 1.4°
250
200
150
100
50
0
10
20
30
40
50
60
70
Channel Number

Figure 8

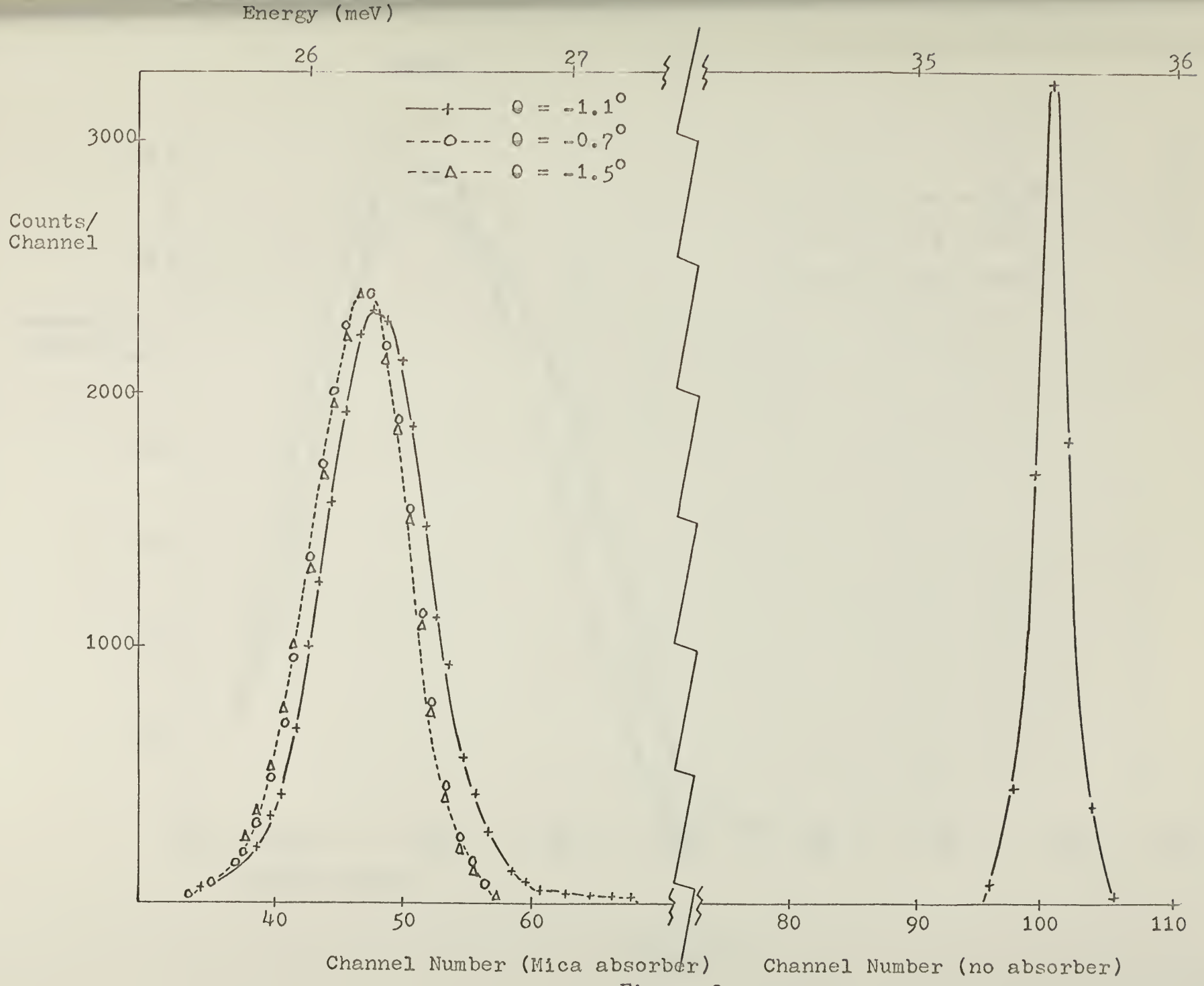
Energy (meV)
26
27
35
36
—+— θ = -1.1°
---o--- θ = -0.7°
---Δ--- θ = -1.5°
3000
2000
1000
Counts/
Channel
40
50
60
80
90
100
110
Channel Number (Mica absorber)
Channel Number (no absorber)

Figure 9

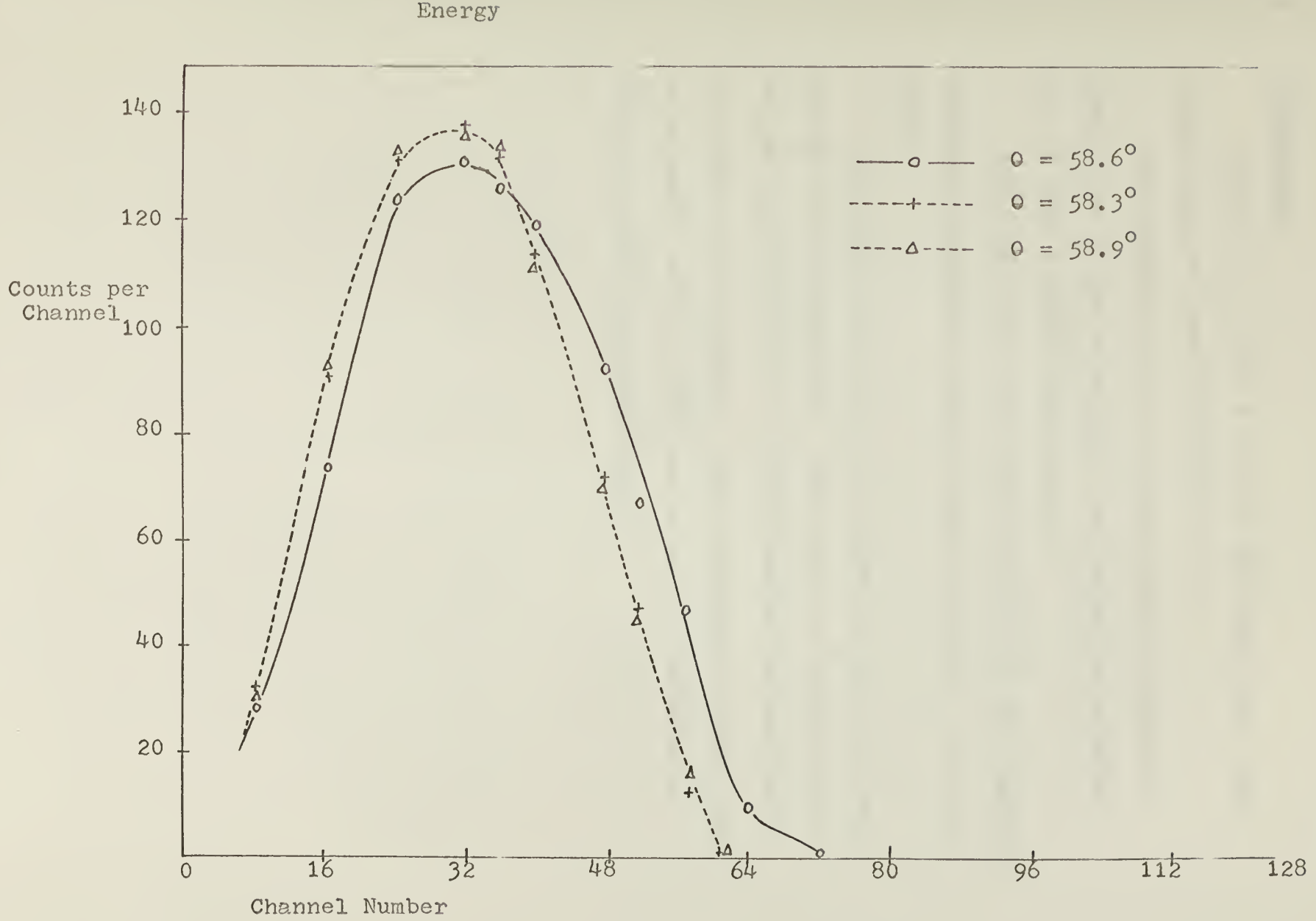
Energy
140
120
Counts per Channel
100
80
60
40
20
0
16
32
48
64
80
96
112
128
Channel Number
θ = 58.6°
θ = 58.3°
θ = 58.9°

Figure 10

Conclusions

Figures 7, 8, and 9 lead to the conclusion that channelling has been observed.

From Table II it can be seen that an empirical prediction of the anisotropy coefficient by equation (3) is only a rough approximation.

Table III shows that the definition of the limiting angle for observable channelling by equation (2) is not exact.

The final conclusion to be drawn is the one stated at the end of Chapter II: The theory of channelling is as yet too inadequate to safely predict the magnitude or extent of the effect. Much experimental effort must be expended before sufficient data are available on which to base a workable theory.

LIST OF REFERENCES

1. J. Silsbee, J. Appl. Phys. 28, 1246(1957).
2. G. R. Piercy, F. Brown, J. A. Davies, and M. McCargo, Phys. Rev. Letters 10, 399(1963).
3. G. R. Piercy, J. A. Davies, M. McCargo, and F. Brown, Bull. Am. Phys. Soc. 8, 196(1963).
4. E. Bogh and C. Uggerhoj, Phys. Letters 12, 116(1964).
5. M. W. Thompson, Phys. Rev. Letters 13, 756(1964).
6. C. Erginsoy, H. E. Wegner, and W. M. Gibson, Phys. Rev. Letters 13, 530(1964).
7. A. R. Sattler and G. Dearnaley, Phys. Rev. Letters 15, 59(1965).
8. S. Datz, T. S. Noggle, and C. D. Moak, Phys. Rev. Letters 15, 254(1964).
9. W. M. Gibson, C. Erginsoy, H. E. Wegner, and B. R. Appleton, Phys. Rev. Letters 15, 357(1965).
10. R. S. Nelson and M. W. Thompson, Phil. Mag. 8, 1677(1963).
11. W. Brandt, J. M. Khan, D. L. Potter, R. D. Worley, and H. P. Smith, Phys. Rev. Letters 14, 42(1965).
12. H. Lutz and R. Sitzmann, Phys. Letters 5, 113(1965).
13. M. T. Robinson and O. S. Oen, Phys. Rev. 132, 2385 (1963).
14. C. Erginsoy, Phys. Rev. Letters 15, 360(1965).
15. J. Lindhard, Phys. Letters 12, 126(1964).
16. W. Whaling, Handbuch der Physik, xxxiv, 13.

BIOGRAPHICAL SKETCH

Griffin F. Hamilton was born at St. Petersburg, Florida on 26 June 1937, the son of a Sergeant Major of Marines. He was graduated from New Hanover High School in Wilmington, North Carolina, in 1955. Upon his graduation from the United States Naval Academy at Annapolis, Maryland, in 1959, he was commissioned an Ensign in the Line of the Navy. He served in destroyers and minecraft of the Pacific Fleet from 1959 to 1964, attaining his present rank of Lieutenant. In 1964 he began graduate study in Electronic Engineering at the United States Naval Postgraduate School, Monterey, California, but was shortly thereafter selected by the Chief of Naval Research to study Physics at the University of Florida under the auspices of the Naval Advanced Science Program.

Lieutenant Hamilton holds the National Defense Service Medal and the Armed Forces Expeditionary Medal (three awards). He is married to the former Katie Ellen Guilford of Washington, D. C., and the father of four sons. He is a member of the United States Naval Institute, and Sigma Pi Sigma national physics honor society, of which he has served as President of the University of Florida chapter.

This thesis was prepared under the direction of the chairman of the candidate's supervisory committee and has been approved by all members of that committee. It was submitted to the Dean of the College of Arts and Sciences and to the Graduate Council, and was approved as partial fulfillment of the requirements for the degree of Master of Science.

August 11, 1966

_____
Dean, College of Arts and Sciences

_____
Dean, Graduate School

_____
Chairman A. R. Quinton

_____
F. E. Dunnam

_____
E. H. Hadlock